J. Fluid Mech. (2014), *vol.* 751, *pp.* 142–163.
doi:10.1017/jfm.2014.294

Effect of large bulk viscosity on large-Reynolds-number flows

M. S. Cramer† and F. Bahmani

Department of Engineering Science and Mechanics, MC 0219, Virginia Polytechnic Institute and State University, Blacksburg, VA 24061, USA

(Received 29 September 2013; revised 28 March 2014; accepted 21 May 2014; first published online 17 June 2014)

We examine the inviscid and boundary-layer approximations in fluids having bulk viscosities which are large compared with their shear viscosities for three-dimensional steady flows over rigid bodies. We examine the first-order corrections to the classical lowest-order inviscid and laminar boundary-layer flows using the method of matched asymptotic expansions. It is shown that the effects of large bulk viscosity are non-negligible when the ratio of bulk to shear viscosity is of the order of the square root of the Reynolds number. The first-order outer flow is seen to be rotational, non-isentropic and viscous but nevertheless slips at the inner boundary. First-order corrections to the boundary-layer flow include a variation of the thermodynamic pressure across the boundary layer and terms interpreted as heat sources in the energy equation. The latter results are a generalization and verification of the predictions of Emanuel (*Phys. Fluids* A, vol. 4, 1992, pp. 491–495).

Key words: aerodynamics, compressible boundary layers, compressible flows

1. Introduction

The inviscid approximation is the foundation of aerodynamics and modern fluid dynamics. In its simplest form it states that most of the flow can be regarded as frictionless and as having negligible heat conduction provided an appropriately defined Reynolds number is sufficiently large. The bulk of the flow is then determined by the Euler equations which are solved subject only to the no-penetration or kinematic boundary condition at material boundaries, e.g. at the surface of solid bodies. The resultant inviscid solutions are the basis of most textbook presentations of fluid mechanics and aerodynamics. In such large-Reynolds-number flows, the no-slip condition is satisfied once a viscous boundary layer forms in the neighbourhood of the solid boundary. Such viscous boundary layers are the physical source of flow vorticity, the Kutta condition, separation, heat transfer and drag. The deceleration of the flow in the boundary layer causes an outward displacement of the flow; this effective thickening of the body, wing or turbine blade is called the displacement thickness effect and plays a key role in the study of viscous–inviscid interactions. The perturbations to the inviscid flow caused by this displacement thickness are of order $Re^{-1/2}$, where Re is the above-mentioned Reynolds number, and are typically

† Email address for correspondence: macramer@vt.edu

inviscid, irrotational and isentropic. The perturbed inviscid flow can then be used to compute the next correction to the boundary layer, which can be used to compute further corrections to the inviscid flow. While the availability of high-speed computers may render such iterative schemes unnecessary for detailed flow computations, the conceptual structure is nevertheless essential for the interpretation of numerical and experimental studies.

The primary goal of the present study is to determine the effect of the bulk viscosity

$$\mu_b \equiv \lambda + \tfrac{2}{3}\mu, \tag{1.1}$$

where μ, λ and μ_b are the shear, second and bulk viscosities of the fluid, on the structure of the inviscid approximation. In particular, we delineate how the inviscid portion of the flow and the boundary layer must be modified when the bulk viscosity is large compared with the shear viscosity. An early study of the bulk viscosity in low-pressure gases has been carried out by Tisza (1942) who showed that the zero-frequency, near-equilibrium value of the bulk viscosity is given by

$$\mu_b = \mu_b(T) = (\gamma - 1)^2 \sum_i \left(\frac{c_v|_i}{R} \right) p\tau_i, \tag{1.2}$$

where T is the absolute temperature, γ is the ratio of specific heats, $c_v|_i$ is the isochoric specific heat corresponding to the ith internal energy storage mode, i.e. the rotational and vibrational modes, R is the gas constant, p is the thermodynamic pressure and τ_i is the relaxation time corresponding to ith mode. The summation is over all of the internal energy storage modes. One of the earliest numerical estimates for the bulk viscosity of an ideal gas was Tisza (1942) who gave a value of $\mu_b/\mu = O(10^3)$ for CO_2 at room temperature and pressure. More recent studies have determined the bulk viscosity for a variety of fluids (see Graves & Argrow 1999; Cramer 2012). In the latter study, a number of common fluids were found to have bulk viscosities which were hundreds to thousands of times larger than their shear viscosities. Examples of the temperature variation of the ratio of bulk to shear viscosity of selected fluids are provided in figure 1. The details of the data used and estimation techniques are provided in Cramer (2012). As discussed by Cramer (2012), fluids having large bulk viscosities include those used as working fluids in power systems having non-fossil fuel heat sources, wind tunnel testing, and pharmaceutical processing. In spite of the prevalence of such fluids in applications, there are very few studies which examine the dynamics of fluids with relatively large bulk viscosities. Recent examples include the work of Emanuel (1992) and Gonzalez & Emanuel (1993). In the first study, the effects of large bulk viscosity on a hypersonic boundary layer were described. In the second study the effect of blowing or suction on a Couette flow of a large bulk viscosity fluid was examined.

In the present study we examine the inviscid flow and boundary layer associated with a steady flow around a rigid three-dimensional smooth body. A sketch of the configuration is provided in figure 2. We include the possibility that the bulk viscosity is much larger than the shear viscosity and describe the corrections required when $\mu_b \gg \mu$. Because the bulk viscosity is proportional to the relaxation times for the internal modes the possibility that the flow will no longer be in equilibrium must be considered. In order to ensure that the Navier–Stokes equations are valid we must require that the flow be near equilibrium, i.e. that $t_g \gg \tau_{max}$, where t_g is the global time scale imposed by the boundary and the initial conditions and τ_{max} is the largest

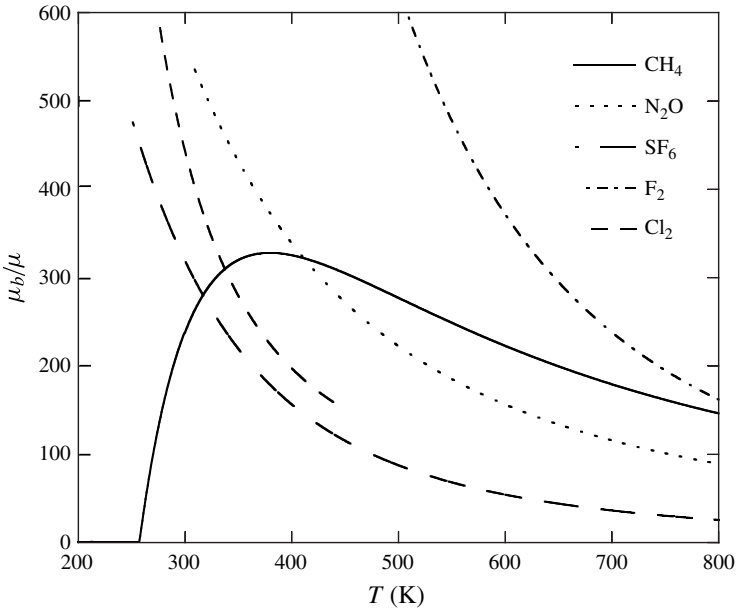

FIGURE 1. Temperature variation of the ratio μ_b/μ for selected fluids. In each case the gas is at low pressure and the bulk viscosity was computed using (1.2) and the data and procedures of Cramer (2012). In the case of methane (CH_4), we have combined the contributions of the rotational and vibrational modes into a single variation.

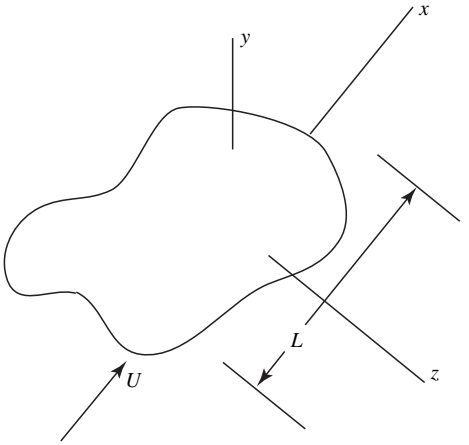

FIGURE 2. Sketch of the coordinate system and configuration.

relevant molecular time scale. Following Graves & Argrow (1999), we refer to this near-equilibrium condition as local thermodynamic equilibrium (LTE). If we formally restrict attention to low-pressure gases and denote the typical molecular collision time as τ_c, the size of the shear viscosity is given by

$$\mu = O(p\tau_c). \tag{1.3}$$

The Reynolds number associated with a body of size L and a freestream speed of U is $Re = U\rho L/\mu$ where ρ is the fluid density. If we note that $t_g = O(L/U)$ and use (1.3), we find that

$$Re = O\left(M_\infty^2 \frac{t_g}{\tau_c}\right) \tag{1.4}$$

where M_∞ is defined as the freestream Mach number. Thus, when the Mach number is of order one, $t_g \gg \tau_c$ for all large Reynolds number flows. However, if we combine (1.2) with (1.3), we find that

$$\frac{\mu_b}{\mu} = O\left(\frac{\tau_i}{\tau_c}\right). \tag{1.5}$$

Thus, for $\mu_b \gg \mu$, $\tau_i \gg \tau_c$ and we need to show that $t_g \gg \tau_i \gg \tau_c$ in order that LTE be satisfied for the flows considered here. An estimate of the size of μ_b/μ needed in the present study can be obtained by recalling that the first correction to classical large Reynolds number, i.e. inviscid, flow is due the displacement thickness effects generated by the boundary layer. As pointed out above, these displacement thickness effects are of order

$$\delta \equiv Re^{-1/2} \ll 1. \tag{1.6}$$

In particular, the perturbations to the thermodynamic pressure due to the displacement thickness are of order $\rho U^2\delta$. The size of the normal component of the viscous part of the stress tensor is of order $\mu_b \boldsymbol{\nabla}\cdot\boldsymbol{v}$, where $\boldsymbol{v}$ is the velocity vector. If we note that $\boldsymbol{\nabla}\cdot\boldsymbol{v} = O(U/L)$, we find that the ratio of (normal) viscous stress to the pressure perturbations associated with displacement thickness is

$$O\left(\mu_b \frac{U}{L}\frac{1}{\rho\delta U^2}\right) = O\left(\frac{\mu_b}{\mu}\frac{1}{\delta Re}\right) = O\left(\frac{\mu_b}{\mu}\frac{1}{Re^{1/2}}\right). \tag{1.7}$$

Thus, the viscous effects associated with the bulk viscosity are on the same order as the correction due to the displacement thickness when

$$\frac{\mu_b}{\mu} = O(Re^{1/2}) = O(\delta^{-1}) \gg 1, \tag{1.8}$$

where (1.6) has been used. If $\mu_b = O(\mu)$, then (1.8) cannot be satisfied and we recover the conclusion of the classical inviscid theory that viscous effects are always much smaller than displacement thickness effects. In all that follows, we employ (1.8) for the sake of convenience. However, we have also derived (1.8) by a detailed and systematic asymptotic analysis of the full Navier–Stokes equations. If we now substitute (1.4) and (1.5) into (1.8) and multiply (1.8) by τ_c/t_g, we find that

$$\frac{\tau_i}{t_g} = O\left(\left(\frac{\tau_c}{t_g}\right)^{1/2}\right) \ll 1, \tag{1.9}$$

where (1.6) and (1.4) have been used. Thus, for the problems considered here, $t_g \gg \tau_i \gg \tau_c$ and LTE is satisfied.

We therefore take the flows to be governed by the Navier–Stokes equations in all that follows. The equations, boundary conditions and flow parameters are provided in § 2. In § 3, we develop the outer approximation to the exact equations to first order

in $Re^{-1/2}$. In § 3 we also describe the vorticity and entropy generated by the non-negligible bulk viscosity. A modified Bernoulli equation, valid to first order, is also reported. In § 4, we find the first-order boundary-layer approximation for sufficiently smooth but otherwise general three-dimensional bodies and flows through use of the curvilinear coordinate system described by Bahmani (2013). The boundary layer is taken to be laminar and attached. In § 5, we match the two first-order approximations using the method of matched asymptotic expansions. Although viscous effects are non-negligible at $O(\delta)$ in the outer flow, the result of the matching is that the first-order outer flow is seen to slip freely at the solid boundary. In § 6, we specialize to the case of a flat plate in order to provide explicit illustrations of the effects of relatively large bulk viscosity on the boundary layer. We verify Emanuel's (1992) result that the pressure is not constant across the boundary layer at first order, but has a $O(Re^{-1/2})$ variation.

2. Formulation

The flow is taken to be steady and such that the body force and volumetric energy supply is negligible. As pointed out in the previous section, the single-phase, non-reacting fluid is taken to be an arbitrary Navier–Stokes fluid. The resultant mass, linear momentum and energy equations can therefore be written

$$\boldsymbol{\nabla}\cdot(\boldsymbol{v}\rho)=0, \tag{2.1}$$

$$\rho\boldsymbol{v}\cdot\boldsymbol{\nabla}\boldsymbol{v}+\boldsymbol{\nabla}p=\boldsymbol{\nabla}\cdot\boldsymbol{T}, \tag{2.2}$$

$$\rho T\boldsymbol{v}\cdot\boldsymbol{\nabla}s=\Phi-\boldsymbol{\nabla}\cdot\boldsymbol{q}, \tag{2.3}$$

where $\boldsymbol{v}=\boldsymbol{v}(\boldsymbol{x})$, $\rho=\rho(\boldsymbol{x})$ and $s=s(\boldsymbol{x})$ are the fluid velocity, density and entropy, and $\boldsymbol{x}$ represents the spatial coordinates. The scalar Φ is the viscous dissipation given by

$$\Phi\equiv\mathrm{tr}(\boldsymbol{T}(\boldsymbol{\nabla}\boldsymbol{v})^{\mathrm{T}}), \tag{2.4}$$

where the superscript T denotes the transpose of the indicated quantity and tr denotes the trace. The heat flux vector ($\boldsymbol{q}$) and the viscous part of the stress tensor ($\boldsymbol{T}$) are given by

$$\boldsymbol{q}\equiv-k\boldsymbol{\nabla}T, \tag{2.5}$$

$$\boldsymbol{T}\equiv\lambda\boldsymbol{\nabla}\cdot\boldsymbol{v}\ \boldsymbol{I}+\mu\left[\boldsymbol{\nabla}\boldsymbol{v}+(\boldsymbol{\nabla}\boldsymbol{v})^{\mathrm{T}}\right], \tag{2.6}$$

where $\boldsymbol{I}$ is the identity matrix and $k=k(\rho,T)$ is the thermal conductivity. The thermodynamic variables are related through Gibbs' relation

$$\mathrm{d}h=T\,\mathrm{d}s+\frac{1}{\rho}\,\mathrm{d}p, \tag{2.7}$$

where

$$h\equiv e+\frac{p}{\rho} \tag{2.8}$$

is the fluid specific enthalpy and $e=e(\rho,T)$ is the fluid energy per unit volume.

It can be shown that the above system is closed once we specify

$$p=p(\rho,T) \tag{2.9}$$

$$c_{v\infty}=c_{v\infty}(T) \tag{2.10}$$

and the dependencies of μ, λ, k on either p and T or ρ and T. The relation (2.9) is recognized as the equation of state and $c_{v\infty} = c_{v\infty}(T)$ is the ideal gas or zero-pressure isochoric specific heat. The constraints on these constitutive properties are that

$$k, \mu, \mu_b \geqslant 0, \tag{2.11}$$

$$c_v = c_v(\rho, T) \equiv T \left.\frac{\partial s}{\partial T}\right|_{\rho} \geqslant 0, \tag{2.12}$$

$$\left.\frac{\partial p}{\partial \rho}\right|_{T} \geqslant 0. \tag{2.13}$$

The first set of inequalities are necessary and sufficient conditions for the Navier–Stokes equations to satisfy the second law of thermodynamics and (2.12) and (2.13) are required in order to ensure a stable thermodynamic equilibrium.

The body is stationary, rigid and impenetrable, but otherwise arbitrary as sketched in figure 2. If the body surface is taken to be $\mathscr{F}(\boldsymbol{x}) = 0$, the combination of no-slip and no-penetration condition at the body surface therefore is

$$\boldsymbol{v} = \boldsymbol{0} \tag{2.14}$$

on $\mathscr{F}(\boldsymbol{x}) = 0$. For either a constant temperature or an adiabatic boundary condition we will take

$$T = T_w = \text{constant} \quad \text{or} \quad \boldsymbol{n} \cdot \boldsymbol{\nabla} T = 0 \tag{2.15a,b}$$

on $\mathscr{F}(\boldsymbol{x}) = 0$ where $\boldsymbol{n}$ is the unit outward normal to the body. Far from the body the flow is taken to be uniform and parallel to the positive x-axis, i.e.

$$\boldsymbol{v} \to U\boldsymbol{i} \quad \text{and} \quad T, p, \to T_\infty, p_\infty, \tag{2.16a,b}$$

as $|\boldsymbol{x}| \to \infty$, where $U = \text{constant}$, $\boldsymbol{i}$ is the unit vector in the positive x direction and subscripts ∞ will always refer to flow properties far from the body.

We now non-dimensionalize the equations of motion as follows

$$\boldsymbol{v} = U\bar{\boldsymbol{v}}, \quad \rho = \rho_\infty \bar{\rho}, \quad p - p_\infty = \rho_\infty U^2 \bar{p}, \tag{2.17a–c}$$

$$T = T_\infty \bar{T}, \quad s - s_\infty = c_{p\infty}\bar{s}, \quad \boldsymbol{x} = L\bar{\boldsymbol{x}}, \quad \boldsymbol{\nabla} = \frac{1}{L}\bar{\boldsymbol{\nabla}}, \tag{2.18a–d}$$

where $c_{p\infty}$ is the specific heat at constant pressure evaluated in the freestream. As a result, (2.1)–(2.3) can be rewritten as

$$\bar{\boldsymbol{\nabla}} \cdot (\bar{\boldsymbol{v}}\bar{\rho}) = 0 \tag{2.19}$$

$$\bar{\rho}\bar{\boldsymbol{v}} \cdot \bar{\boldsymbol{\nabla}}\bar{\boldsymbol{v}} + \bar{\boldsymbol{\nabla}}\left[\bar{p} - \frac{\bar{\mu}_b}{Re}\bar{\boldsymbol{\nabla}} \cdot \bar{\boldsymbol{v}}\right] = \frac{1}{Re}\bar{\boldsymbol{\nabla}} \cdot \bar{\boldsymbol{T}}_0 \tag{2.20}$$

$$\bar{\rho}\bar{T}\bar{\boldsymbol{v}} \cdot \bar{\boldsymbol{\nabla}}\bar{s} = \frac{1}{Re}\left[E\left(\bar{\Phi}_0 + \bar{\mu}_b(\bar{\boldsymbol{\nabla}} \cdot \bar{\boldsymbol{v}})^2\right) - \frac{1}{Pr}\bar{\boldsymbol{\nabla}} \cdot \bar{\boldsymbol{q}}\right]. \tag{2.21}$$

The boundary conditions (2.14)–(2.16) can be written

$$\bar{\boldsymbol{v}} = \boldsymbol{0}, \quad \bar{T} = \bar{T}_w = \text{constant} \quad \text{or} \quad \boldsymbol{n} \cdot \bar{\boldsymbol{\nabla}}\bar{T} = 0 \tag{2.22a–c}$$

on $\mathscr{F}(\bar{\boldsymbol{x}}) = 0$ and

$$\bar{\boldsymbol{v}} \to \boldsymbol{i} \quad \bar{\rho}, \bar{T} \to 1 \quad \bar{p}, \bar{s} \to 0 \tag{2.23a–c}$$

as $|\bar{\boldsymbol{x}}| \to \infty$. Here $Re \equiv U\rho_\infty L/\mu_\infty$, $Pr = \mu_\infty c_{p\infty}/k_\infty$, $E = U^2/T_\infty c_{p\infty}$ are the Reynolds number, Prandtl number and Eckert number. The quantities μ_∞ and k_∞ are the shear viscosity and thermal conductivity evaluated in the freestream. The quantities

$$\bar{\boldsymbol{q}} \equiv -\bar{k}\bar{\boldsymbol{\nabla}}\bar{T} = \frac{L}{k_\infty T_\infty}\boldsymbol{q}, \tag{2.24}$$

$$\bar{\boldsymbol{T}} = \bar{\boldsymbol{T}}_0 + \bar{\mu}_b\bar{\boldsymbol{\nabla}}\cdot\bar{\boldsymbol{v}}\ \boldsymbol{I} \equiv \frac{L}{U\mu_\infty}\boldsymbol{T}, \tag{2.25}$$

$$\bar{\Phi} = \bar{\Phi}_0 + \bar{\mu}_b(\bar{\boldsymbol{\nabla}}\cdot\bar{\boldsymbol{v}})^2 = \frac{L^2}{\mu_\infty U^2}\Phi, \tag{2.26}$$

are the scaled versions of (2.5), (2.6) and (2.4), respectively. The non-dimensional thermal conductivity, viscosity and bulk viscosity are defined as follows: $\bar{k} \equiv k/k_\infty$, $\bar{\mu} \equiv \mu/\mu_\infty$ and $\bar{\mu}_b \equiv \mu_b/\mu_\infty$. In (2.24)–(2.26) we have split the shear stress and viscous dissipation into the $\mu_b = 0$ contribution, i.e.

$$\bar{\boldsymbol{T}}_0 = \bar{\mu}\left[\bar{\boldsymbol{\nabla}}\bar{\boldsymbol{v}} + \left(\bar{\boldsymbol{\nabla}}\bar{\boldsymbol{v}}\right)^{\mathrm{T}} - \tfrac{2}{3}\bar{\boldsymbol{\nabla}}\cdot\bar{\boldsymbol{v}}\ \boldsymbol{I}\right], \tag{2.27}$$

$$\bar{\Phi}_0 = \mathrm{tr}\left[\bar{\boldsymbol{T}}_0(\bar{\boldsymbol{\nabla}}\bar{\boldsymbol{v}})^{\mathrm{T}}\right], \tag{2.28}$$

and the $\mu_b \neq 0$ contributions. Equation (2.27) can also be recognized as the non-dimensionalized version of the deviatoric viscous stress tensor. In all that follows we will take the Reynolds number to be large, the Prandtl and Eckert numbers to be of order one, and $\bar{\mu}_b = O(Re^{1/2}) \gg 1$.

3. Outer solution

We now seek approximations to (2.19)–(2.21) for the lowest-order outer flow as well as its first correction by expanding the dependent variables as follows:

$$\left.\begin{aligned}
\bar{\boldsymbol{v}} &= \boldsymbol{V}_0 + \delta\boldsymbol{V}_1 + O(\delta^2),\\
\bar{p} &= P_0 + \delta P_1 + O(\delta^2),\\
\bar{T} &= T_0 + \delta T_1 + O(\delta^2),\\
\bar{\rho} &= R_0 + \delta R_1 + O(\delta^2),\\
\bar{s} &= S_0 + \delta S_1 + O(\delta^2),
\end{aligned}\right\} \tag{3.1}$$

where

$$\delta \equiv Re^{-1/2} \ll 1, \tag{3.2}$$

and $\bar{\mu}_b = O(\delta^{-1})$. In the outer flow each component of $\bar{\boldsymbol{x}} = O(1)$ and, in anticipation of the existence of the boundary layer, we ignore the boundary conditions at $\mathscr{F}(\bar{\boldsymbol{x}}) = 0$. Substitution of (3.1) in (2.19)–(2.21) yields

$$\bar{\boldsymbol{\nabla}}\cdot(\tilde{\rho}\tilde{\boldsymbol{v}}) = O(\delta^2), \tag{3.3}$$

$$\tilde{\rho}\tilde{\boldsymbol{v}}\cdot\bar{\boldsymbol{\nabla}}\tilde{\boldsymbol{v}} + \bar{\boldsymbol{\nabla}}\left[\tilde{p} - \bar{\mu}_b\delta^2\bar{\boldsymbol{\nabla}}\cdot\tilde{\boldsymbol{v}}\right] = O(\delta^2), \tag{3.4}$$

$$\tilde{\boldsymbol{v}}\cdot\bar{\boldsymbol{\nabla}}\tilde{s} = E\frac{\bar{\mu}_b\delta^2}{\tilde{\rho}\tilde{T}}\left(\bar{\boldsymbol{\nabla}}\cdot\tilde{\boldsymbol{v}}\right)^2 + O(\delta^2), \tag{3.5}$$

where symbols with tildes denote the first two terms in (3.1), e.g. $\tilde{\boldsymbol{v}} \equiv \boldsymbol{V}_0 + \delta\boldsymbol{V}_1$, $\tilde{p} \equiv P_0 + \delta P_1$, etc., in order to simplify the appearance of (3.3)–(3.5). It should be noted

that terms explicitly recorded in (3.3)–(3.5) will also contain terms which are of $O(\delta^2)$ and such terms should be ignored when more detailed expansions are carried out. We also note that the lowest-order version of (3.3)–(3.5) can be written

$$\bar{\nabla} \cdot (R_0 \boldsymbol{V}_0) = 0, \tag{3.6}$$

$$R_0 \boldsymbol{V}_0 \cdot \bar{\nabla} \boldsymbol{V}_0 + \bar{\nabla} P_0 = \boldsymbol{0}, \tag{3.7}$$

$$\boldsymbol{V}_0 \cdot \bar{\nabla} S_0 = 0, \tag{3.8}$$

which are recognized as the classical equations governing inviscid isentropic flow. When $\bar{\mu}_b = O(1)$, (3.3)–(3.5) also reduce to the equations of inviscid, isentropic flow. Thus, in the classical $\bar{\mu}_b = O(1)$ theory, the $O(\delta)$ perturbations are caused only by the boundary-layer displacement thickness. In the present case, we take $\bar{\mu}_b = O(\delta^{-1})$ and the viscous terms proportional to $\bar{\mu}_b$ are non-negligible at first order. That is, first-order corrections to the outer flow are due to both classical displacement thickness effects and (bulk) viscous effects when $\bar{\mu}_b = O(Re^{1/2}) = O(\delta^{-1})$. The viscous effects are seen to be related to the compressibility of the lowest-order inviscid flow, i.e.

$$\bar{\nabla} \cdot \tilde{\boldsymbol{v}} \approx \bar{\nabla} \cdot \boldsymbol{V}_0 \approx -\frac{1}{R_0} \boldsymbol{V}_0 \cdot \nabla R_0 \tag{3.9}$$

and can be ignored if the lowest-order outer flow is incompressible.

The far-field boundary conditions (2.23) reduce to

$$\tilde{\boldsymbol{V}} \to \boldsymbol{i}, \quad \tilde{\rho} \to 1, \quad \tilde{T} \to 1, \quad \tilde{p} \to 0, \quad \tilde{s} \to 0 \tag{3.10a–e}$$

as $|\bar{\boldsymbol{x}}| \to \infty$. By combining (3.8) and the last of (3.10), we can show that $S_0 = 0$ for all $\bar{\boldsymbol{x}}$ and that S_1 is given by (3.5):

$$\boldsymbol{V}_0 \cdot \bar{\nabla} S_1 = E \frac{\bar{\mu}_b \delta}{R_0 T_0} \left(\bar{\nabla} \cdot \boldsymbol{V}_0 \right)^2. \tag{3.11}$$

Thus, when $\bar{\mu}_b = O(\delta^{-1})$, $\bar{s} = O(\delta)$ in the outer flow and the perturbations caused by the displacement thickness are not only viscous but involve entropy gradients even in a shock-free flow.

The outer flow is also seen to be rotational at the order of the displacement thickness corrections. This fact can be seen by taking the curl of (3.4), by using well-known vector identities and the thermodynamic identity

$$\left. \frac{\partial p}{\partial s} \right|_{\rho} = \rho T G, \tag{3.12}$$

where $G \equiv \beta a^2 / c_p$ is the Grüneisen parameter and

$$\beta \equiv -\frac{1}{\rho} \left. \frac{\partial \rho}{\partial T} \right|_{p} \tag{3.13}$$

is the thermal expansivity, to yield a modified version of the vorticity transport equation. In terms of the dimensional variables this modified vorticity transport equation reads

$$\boldsymbol{v} \cdot \nabla \boldsymbol{\omega} \approx \boldsymbol{\omega} \cdot \nabla \boldsymbol{v} + \frac{1}{\rho^2} \nabla \rho \times [GT \nabla s - \nabla(\Delta)] \tag{3.14}$$

where $\boldsymbol{\omega} \equiv \boldsymbol{\zeta}/\rho$, $\boldsymbol{\zeta} \equiv \boldsymbol{\nabla} \times \boldsymbol{v}$ = vorticity, and

$$\Delta \equiv \nu_b \boldsymbol{\nabla} \cdot \boldsymbol{v}, \tag{3.15}$$

where $\nu_b \equiv \mu_b/\rho$ is the kinematic bulk viscosity. The accuracy of (3.14) is identical to that of (3.3)–(3.5), i.e. the terms neglected in (3.14) are $O(U^2\delta^2/L^2\rho_\infty)$. The term on the left-hand side of (3.14) is the time variation of $\boldsymbol{\omega}$ on a particle path, the first term on the right-hand side of (3.14) is the vortex stretching term and the term proportional to $\boldsymbol{\nabla}\rho \times \boldsymbol{\nabla} s$ is the baroclinic vorticity generation term found in the classical inviscid version of the vorticity transport equation. The term proportional to $\boldsymbol{\nabla}\rho \times \boldsymbol{\nabla}(\Delta)$ arises due to the first-order viscous term in (3.4). Because the dimensional entropy variations are of order $\delta c_{p\infty}$, the last two terms in (3.14) can be shown to be of first order when $\bar{\mu}_b = O(\delta^{-1})$. Thus, in the case considered here, i.e. $\bar{\mu}_b = O(\delta^{-1})$, the last two terms on the right-hand side of (3.14) will be $O(U^2\delta/L^2\rho_\infty)$ and the first-order outer flow will be rotational, i.e.

$$\boldsymbol{\zeta} = O\left(\delta \frac{U}{L}\right). \tag{3.16}$$

The first-order vorticity is seen to be due to the entropy gradients caused by viscous dissipation term in (3.5) and the viscous term seen in the momentum equation (3.4).

A modified Bernoulli equation can be derived by dotting (3.4) with $\tilde{\boldsymbol{v}}$ and by using standard vector identities, Gibbs' relation (2.7) and (3.5). In dimensional variables, this modified Bernoulli equation reads

$$h + \frac{|\boldsymbol{v}|^2}{2} - \Delta \approx \text{constant} \tag{3.17}$$

on particle paths, where Δ is again given by (3.15). Here, the terms neglected in (3.17) are $O(U^2\delta^2)$. It can be shown that the shock jump conditions are the classical jump conditions with the pressure replaced by $p - \mu_b \boldsymbol{\nabla} \cdot \boldsymbol{v} = p - \rho\Delta$, at least to first order. As a result, (3.17) holds along all particle paths, including those which pass through shock waves. If we employ the boundary conditions (3.10), we conclude that

$$H - H_\infty \approx \Delta \tag{3.18}$$

for all particle paths even when shock waves are present. Here $H \equiv h + |\boldsymbol{v}|^2/2$ is the total enthalpy and $H_\infty \equiv h_\infty + U^2/2$. Due to (2.11) $\nu_b > 0$ which implies

$$H \gtrless H_\infty \text{ wherever } \boldsymbol{\nabla} \cdot \boldsymbol{v} = -\frac{1}{\rho} \boldsymbol{v} \cdot \boldsymbol{\nabla}\rho \gtrless 0, \tag{3.19}$$

i.e. the total enthalpy exceeds the freestream total enthalpy in all regions where the density is decreasing along the streamline and is less than the freestream enthalpy in all regions where the density is increasing along the streamline. At stagnation points, $\boldsymbol{v} = \boldsymbol{0}$ and the stagnation enthalpy is

$$h_s = H_\infty. \tag{3.20}$$

Because the entropy increases along every streamline due both to shock waves and the first-order energy equation (3.5), Gibbs' relation (2.7) can be used to show that the stagnation pressure, i.e. the pressure at a stagnation point, will be less than the pressure obtained during an isentropic stagnation.

4. Inner solution

We now analyse the boundary layer using a surface-oriented coordinate system defined by

$$\boldsymbol{x} = \boldsymbol{f}(\phi_1, \phi_2) + n\boldsymbol{n}, \tag{4.1}$$

where the body sketched in figure 2 is given by $\boldsymbol{x} = \boldsymbol{f}(\phi_1, \phi_2)$ and ϕ_1, ϕ_2 are the surface parameters. The unit normal to the body pointing out of the body is $\boldsymbol{n} = \boldsymbol{n}(\phi_1, \phi_2)$ and the distance measured normal to the body is given by n. The three-dimensional curvilinear system is orthogonal if and only if the surface coordinate lines are aligned with the principal directions on the surface; in all that follows we take that to be the case. The distances along the ϕ_1, ϕ_2, n coordinate lines are ξ_1, ξ_2, n which satisfy

$$\mathrm{d}\xi_1 = h_1\,\mathrm{d}\phi_1, \quad \mathrm{d}\xi_2 = h_2\mathrm{d}\phi_2, \quad \mathrm{d}n, \tag{4.2a–c}$$

where

$$h_1 = a_1\left(1 + \frac{n}{\mathscr{R}_1}\right), \quad h_2 = a_2\left(1 + \frac{n}{\mathscr{R}_2}\right) \tag{4.3a,b}$$

are the scale factors of the three-dimensional curvilinear system, $a_1 = a_1(\phi_1, \phi_2)$, $a_2 = a_2(\phi_1, \phi_2)$ are the surface scale factors equal to the square root of the diagonal elements of the surface metric and $\mathscr{R}_1 \equiv \mathscr{R}_1(\phi_1, \phi_2)$, $\mathscr{R}_2 \equiv \mathscr{R}_2(\phi_1, \phi_2)$ are the principal radii of curvature of the body surface. The exact steady flow Navier–Stokes equations (2.1)–(2.6) were then written in terms of the system (4.1); the details of the recast exact equations can be found in Bahmani (2013).

We now rescale the independent variables as follows

$$\xi_1 = L\bar{\xi}_1, \quad \xi_2 = L\bar{\xi}_2, \quad n = \delta L\hat{n} \tag{4.4a–c}$$

and the curvilinear velocity components v_1, v_2, v_3 as follows

$$v_1 = Uu, \quad v_2 = Uv, \quad v_3 = \delta Uw, \tag{4.5a–c}$$

where $u, v, w, \bar{\xi}_1, \bar{\xi}_2, \hat{n}$ will be taken to be $O(1)$ in the boundary layer. The remaining dependent variables have the same scalings as in (2.18), i.e. $\rho = \rho_\infty\bar{\rho}$, $p - p_\infty = \rho_\infty U^2\bar{p}$, $T = T_\infty\bar{T}$, $s - s_\infty = c_{p\infty}\bar{s}$. The resultant first-order mass, momentum and energy equations can then be written

$$\frac{\partial(\bar{\rho}u)}{\partial\bar{\xi}_1} + \frac{\partial(\bar{\rho}v)}{\partial\bar{\xi}_2} + \frac{\partial(\bar{\rho}w)}{\partial\hat{n}} + \bar{\rho}u\bar{\alpha}_{21} + \bar{\rho}v\bar{\alpha}_{12} + \delta w\bar{\rho}\left(\frac{1}{\bar{\mathscr{R}}_1} + \frac{1}{\bar{\mathscr{R}}_2}\right) = O(\delta^2) \tag{4.6}$$

$$\bar{\rho}\left[\widehat{\boldsymbol{v}\cdot\boldsymbol{\nabla}}u + vu\bar{\alpha}_{12} - (v)^2\bar{\alpha}_{21} + \frac{\delta wu}{\bar{\mathscr{R}}_1}\right] + \frac{\partial}{\partial\bar{\xi}_1}\left(\bar{p} - \delta\bar{\rho}\hat{\Delta}\right)$$
$$= \frac{\partial\hat{T}_{31}}{\partial\hat{n}} + \delta\hat{T}_{31}\left(\frac{2}{\bar{\mathscr{R}}_1} + \frac{1}{\bar{\mathscr{R}}_2}\right) + O(\delta^2) \tag{4.7}$$

$$\bar{\rho}\left[\widehat{\boldsymbol{v}\cdot\boldsymbol{\nabla}}v + uv\bar{\alpha}_{21} - (u)^2\bar{\alpha}_{12} + \delta\frac{vw}{\bar{\mathscr{R}}_2}\right] + \frac{\partial}{\partial\bar{\xi}_2}\left(\bar{p} - \delta\bar{\rho}\hat{\Delta}\right)$$
$$= \frac{\partial\hat{T}_{32}}{\partial\hat{n}} + \delta\hat{T}_{32}\left[\frac{1}{\bar{\mathscr{R}}_1} + \frac{2}{\bar{\mathscr{R}}_2}\right] + O(\delta^2) \tag{4.8}$$

$$\frac{\partial}{\partial\hat{n}}\left[\bar{p} - \delta\bar{\rho}\hat{\Delta}\right] = \delta\bar{\rho}\left[\frac{(u)^2}{\bar{\mathscr{R}}_1} + \frac{(v)^2}{\bar{\mathscr{R}}_2}\right] + O(\delta^2), \tag{4.9}$$

$$\bar{\rho}\bar{T}\widehat{\boldsymbol{v}\cdot\nabla}\bar{s} = E\left[\hat{\Phi}_0 + \delta\bar{\rho}\hat{\Delta}\widehat{\nabla\cdot\boldsymbol{v}}\right] - \frac{1}{Pr}\widehat{\nabla\cdot\boldsymbol{q}} + O(\delta^2), \tag{4.10}$$

where $\bar{\mathscr{R}}_1 = \mathscr{R}_1/L = O(1)$, $\bar{\mathscr{R}}_2 = \mathscr{R}_2/L = O(1)$,

$$\bar{\alpha}_{21} \equiv \frac{L}{h_1 h_2}\frac{\partial h_2}{\partial \phi_1} = O(1) \tag{4.11}$$

$$\bar{\alpha}_{12} \equiv \frac{L}{h_1 h_2}\frac{\partial h_1}{\partial \phi_2} = O(1). \tag{4.12}$$

The quantity

$$\widehat{\boldsymbol{v}\cdot\nabla}A \equiv \frac{L}{U}\boldsymbol{v}\cdot\nabla A = u\frac{\partial A}{\partial \bar{\xi}_1} + v\frac{\partial A}{\partial \bar{\xi}_2} + w\frac{\partial A}{\partial \hat{n}}, \tag{4.13}$$

where A is any scalar and the scaled divergence of $\boldsymbol{v}$ and $\boldsymbol{q}$ are given by

$$\widehat{\nabla\cdot\boldsymbol{v}} = \frac{\partial u}{\partial \bar{\xi}_1} + \frac{\partial v}{\partial \bar{\xi}_2} + \frac{\partial w}{\partial \hat{n}} + v\bar{\alpha}_{12} + u\bar{\alpha}_{21} + \delta w\left(\frac{1}{\bar{\mathscr{R}}_1} + \frac{1}{\bar{\mathscr{R}}_2}\right) + O(\delta^2), \tag{4.14}$$

$$\widehat{\nabla\cdot\boldsymbol{q}} = -\left[\frac{\partial}{\partial \hat{n}}\left(\bar{k}\frac{\partial \bar{T}}{\partial \hat{n}}\right) + \delta\bar{k}\left(\frac{1}{\bar{\mathscr{R}}_1} + \frac{1}{\bar{\mathscr{R}}_2}\right)\frac{\partial \bar{T}}{\partial \hat{n}}\right] + O(\delta^2). \tag{4.15}$$

The quantity $\hat{\Delta}$ is the scaled version of (3.15), i.e.

$$\hat{\Delta} = \frac{\rho_\infty L}{\mu_\infty U}\delta\Delta = \delta\frac{\bar{\mu}_b}{\bar{\rho}}\widehat{\nabla\cdot\boldsymbol{v}} = O(1). \tag{4.16}$$

The scaled components of the stress tensor are given by

$$\hat{T}_{31} = 2\bar{\mu}\hat{D}_{31}, \quad \hat{T}_{32} = 2\bar{\mu}\hat{D}_{32} \tag{4.17a,b}$$

and the scaled components of the stretching tensor are

$$\left.\begin{aligned}\hat{D}_{31} &= \frac{1}{2}\left(\frac{\partial u}{\partial \hat{n}} - \frac{\delta u}{\bar{\mathscr{R}}_1}\right) + O(\delta^2)\\ \hat{D}_{32} &= \frac{1}{2}\left(\frac{\partial v}{\partial \hat{n}} - \frac{\delta v}{\bar{\mathscr{R}}_2}\right) + O(\delta^2).\end{aligned}\right\} \tag{4.18}$$

The rescaled version of (2.28) is

$$\hat{\Phi}_0 = 4\bar{\mu}\left[(\hat{D}_{31})^2 + (\hat{D}_{32})^2\right] + O(\delta^2). \tag{4.19}$$

The scaled versions of the boundary conditions at the body surface are

$$u = v = w = 0 \tag{4.20}$$

and either

$$\bar{T} = \bar{T}_w = T_w/T_\infty = \text{constant for an isothermal body} \tag{4.21}$$

or

$$\frac{\partial \bar{T}}{\partial \hat{n}} = 0 \quad \text{for an adiabatic body} \tag{4.22}$$

on $\hat{n} = 0$.

Inspection of the mass, momentum and energy equations (4.6)–(4.10) reveals that the primary change to the $\mu_b = O(\mu)$ first-order boundary-layer equations is the replacement of the negative pressure by the normal stresses T_{11}, T_{22} or T_{33} which are $\approx -p + \mu_b(\boldsymbol{\nabla}\cdot\boldsymbol{v})$ when $\mu_b = O(\mu/\delta) = O(\mu Re^{1/2})$. Similar conclusions can be made for the first-order outer flow.

The energy equation (4.10) can be recast as an equation for the temperature through use of the $T\,\mathrm{d}s$ equation

$$T\,\mathrm{d}s = c_p\,\mathrm{d}T - \frac{\beta T}{\rho}\,\mathrm{d}p, \tag{4.23}$$

and the mass equation (4.3) to yield

$$\begin{aligned}\bar{\rho}\bar{c}_p\widehat{\boldsymbol{v}\cdot\boldsymbol{\nabla}}\bar{T} \;=\; & E\hat{\Phi}_0 + ET\beta\widehat{\boldsymbol{v}\cdot\boldsymbol{\nabla}}(\bar{p}-\delta\bar{\rho}\hat{\Delta}) + \delta E\left[(\beta T-1)\widehat{\boldsymbol{v}\cdot\boldsymbol{\nabla}}(\bar{\rho}\hat{\Delta}) + \widehat{\boldsymbol{\nabla}\cdot(\boldsymbol{v}\bar{\rho}\hat{\Delta})}\right]\\ & - \frac{1}{Pr}\widehat{\boldsymbol{\nabla}\cdot\boldsymbol{q}} + O(\delta^2),\end{aligned} \tag{4.24}$$

where

$$\widehat{\boldsymbol{\nabla}\cdot(\boldsymbol{v}\bar{\rho}\hat{\Delta})} = \frac{\partial(u\bar{\rho}\hat{\Delta})}{\partial\bar{\xi}_1} + \frac{\partial(v\bar{\rho}\hat{\Delta})}{\partial\bar{\xi}_2} + \frac{\partial(w\bar{\rho}\hat{\Delta})}{\partial\hat{n}} + \bar{\rho}\hat{\Delta}\,(u\bar{\alpha}_{21} + v\bar{\alpha}_{12}) + O(\delta). \tag{4.25}$$

The quantity (4.25) is just a scaled version of $\boldsymbol{\nabla}\cdot(\boldsymbol{v}\rho\Delta)$ and is the scaled, steady-state version of Emanuel's function F (Emanuel 1992). As in (4.7)–(4.9), the pressure appears only as the normal stress $-\bar{p} + \delta\bar{\rho}\hat{\Delta}$. Except for this modified pressure, the only contribution of the large bulk viscosity are the third and fourth terms on the right-hand side of (4.24). The third term will affect the flow if and only if the fluid is a non-ideal, i.e. pressurized, gas. The fourth term will always contribute when the lowest-order boundary layer flow is compressible. Both the third and fourth terms on the right-hand side of (4.24) can be regarded as heat sources for the first-order problem.

Ordinarily, we would further expand the dependent variables as follows

$$\left.\begin{aligned} u &= u_0(\bar{\xi}_1,\bar{\xi}_2,\hat{n}) + \delta u_1(\bar{\xi}_1,\bar{\xi}_2,\hat{n}) + O(\delta^2)\\ v &= v_0(\bar{\xi}_1,\bar{\xi}_2,\hat{n}) + \delta v_1(\bar{\xi}_1,\bar{\xi}_2,\hat{n}) + O(\delta^2),\\ w &= w_0(\bar{\xi}_1,\bar{\xi}_2,\hat{n}) + \delta w_1(\bar{\xi}_1,\bar{\xi}_2,\hat{n}) + O(\delta^2),\\ \bar{\rho} &= \rho_0(\bar{\xi}_1,\bar{\xi}_2,\hat{n}) + \delta\rho_1(\bar{\xi}_1,\bar{\xi}_2,\hat{n}) + O(\delta^2),\\ \bar{p} &= p_0(\bar{\xi}_1,\bar{\xi}_2,\hat{n}) + \delta p_1(\bar{\xi}_1,\bar{\xi}_2,\hat{n}) + O(\delta^2),\\ \bar{T} &= \theta_0(\bar{\xi}_1,\bar{\xi}_2,\hat{n}) + \delta\theta_1(\bar{\xi}_1,\bar{\xi}_2,\hat{n}) + O(\delta^2). \end{aligned}\right\} \tag{4.26}$$

Although we will use the explicit expansions (3.1) and (4.26) in the next section, here we will simply regard the variables seen in (4.6)–(4.10) and associated equations as representing the first two terms of the expansions (4.26). A similar grouping of terms was convenient in the examination of the outer flow in § 3.

5. Matching

We now establish the boundary conditions for the outer flow at the inner boundary, i.e. the body surface, and the boundary conditions satisfied by the boundary-layer

variables as the outer flow is approached using the method of matched asymptotic expansions (Van Dyke 1964). The matching will be carried out in the curvilinear coordinate system described in § 4 and Bahmani (2013). The independent variables in the outer region of § 3 will be taken to be $\bar{\xi}_1, \bar{\xi}_2, \bar{n} \equiv n/L = \delta\hat{n}$ and the independent variables in the boundary layer will be taken to be $\bar{\xi}_1, \bar{\xi}_2, \hat{n} \equiv \bar{n}/\delta$. The velocity components in the outer region will be written

$$\left.\begin{aligned} \bar{v}_1 &= U_0(\bar{\xi}_1, \bar{\xi}_2, \bar{n}) + \delta U_1(\bar{\xi}_1, \bar{\xi}_2, \bar{n}) + O(\delta^2) \\ \bar{v}_2 &= V_0(\bar{\xi}_1, \bar{\xi}_2, \bar{n}) + \delta V_1(\bar{\xi}_1, \bar{\xi}_2, \bar{n}) + O(\delta^2) \\ \bar{v}_3 &= W_0(\bar{\xi}_1, \bar{\xi}_2, \bar{n}) + \delta W_1(\bar{\xi}_1, \bar{\xi}_2, \bar{n}) + O(\delta^2) \end{aligned}\right\} \tag{5.1}$$

and the remaining dependent variables will be given by the forms seen in (3.1) with independent variables taken to be $\bar{\xi}_1, \bar{\xi}_2, \bar{n}$.

Here we will simply summarize the results of the formal matching of the first-order outer solution to the first-order boundary layer solution. The details of the matching of the 1, 2 components of the velocity and the pressure, density and temperature are essentially the same and result in constraints on the boundary-layer solution only. These constraints can be shown to be identical to the $\mu_b = O(\mu)$ theory to first order. In particular, the 1, 2 components of the velocities in the outer region are not constrained. As a result, the outer flow will be permitted to slip at the body surface, i.e. as $\bar{n} \to 0$, even though viscous effects are non-negligible at first order when $\overline{\mu}_b = O(\delta^{-1})$. As in the $\mu_b = O(\mu)$ theory the boundary-layer variables simply approach the inner limit of those of the outer flow. These matching conditions provide boundary conditions for the solution to (4.6)–(4.10). For example, the pressure perturbations in (4.26) were found to satisfy

$$p_0(\bar{s}_1, \bar{s}_2, \hat{n}) \sim P_0(\bar{\xi}_1, \bar{\xi}_2, 0) + o(1) \tag{5.2}$$

and

$$p_1(\bar{\xi}_1, \bar{\xi}_2, \hat{n}) \sim \hat{n}\frac{\partial P_0}{\partial \bar{n}}(\bar{\xi}_1, \bar{\xi}_2, 0) + P_1(\bar{\xi}_1, \bar{\xi}_2, 0) + o(1) \tag{5.3}$$

as $\hat{n} \to \infty$ with similar expressions for u_0, v_0, ρ_0, θ_0, u_1, v_1, ρ_1 and θ_1. Here P_0, P_1 are computed from the lowest-order and first-order outer solutions. The boundary conditions (5.2) and (5.3) will play a key role in § 6. The matching of the normal component of velocity proceeds slightly differently and yields different results due to the fact that $v_3 = O(U\delta)$ in the boundary layer and $v_3 = O(U)$ in the outer flow. The result of this matching yields

$$\left.\begin{aligned} W_0(\bar{\xi}_1, \bar{\xi}_2, 0) &= 0 \\ W_1(\bar{\xi}_1, \bar{\xi}_2, 0) &= \lim_{\hat{n}\to\infty}\left\{ w_0(\bar{\xi}_1, \bar{\xi}_2, \hat{n}) - \hat{n}\frac{\partial W_0}{\partial \bar{n}}(\bar{\xi}_1, \bar{\xi}_2, 0)\right\}. \end{aligned}\right\} \tag{5.4}$$

The first of (5.4) requires that the lowest-order outer flow satisfies the no-penetration condition and the second condition of (5.4) provides the $O(\delta)$ perturbation leading to boundary-layer displacement thickness effects. If we compare the above conditions to those obtained in the classical, i.e. $\mu_b = O(\mu)$, boundary-layer theory, we see that the primary difference, at least in the present context, is the addition of the normal

stress $\mu_b(\nabla \cdot \boldsymbol{v})$ to the equations of motion. Furthermore, the general procedure for the computation of the higher-order corrections to the inner and outer flows is essentially unchanged.

6. Flat plate boundary layer

In this section we determine the simplification to the boundary-layer equations (4.6)–(4.9) and (4.24) possible when we restrict the flow to be two-dimensional and over a flat plate. The condition of two-dimensional flow requires that all derivatives in the ϕ_2 direction are zero and that $v = 0$. For such a two-dimensional flat plate we can show that

$$a_1 = a_2 = 1 \quad \text{and} \quad \mathscr{R}_1, \mathscr{R}_2 \to \infty, \tag{6.1a,b}$$

from which we conclude that $h_1 = h_2 = 1$ and $\overline{\alpha}_{12} = \overline{\alpha}_{21} = 0$. Thus, (4.9) can be integrated to yield

$$\bar{p} - \delta \bar{\rho} \hat{\Delta} = \text{function of } \bar{\xi} \text{ only}, \tag{6.2}$$

where we have written $\bar{\xi} = \bar{\xi}_1$. For a two-dimensional flow over a flat plate, the lowest-order outer flow solution can be written

$$P_0, S_0 = 0, \quad R_0 = T_0 = 1, \quad \boldsymbol{V}_0 = \boldsymbol{i} \tag{6.3a–c}$$

where $\boldsymbol{i}$ is the unit base vector parallel to the plate. The matching condition on the pressure (5.2) and (5.3) yields

$$\bar{p} \sim \delta P_1(\bar{\xi}, 0) \quad \text{as } \hat{n} \to \infty. \tag{6.4}$$

The matching conditions on velocity and density along with the mass equation (4.6) yields

$$\hat{\Delta} \to 0 \quad \text{as } \hat{n} \to \infty. \tag{6.5}$$

Thus, by combining (6.2), (6.4) and (6.5) we find that

$$\bar{p} = \delta[P_1(\bar{\xi}, 0) + \bar{\rho}\hat{\Delta}] + O(\delta^2) \tag{6.6}$$

for all $\bar{\xi}$, $\hat{n}$. Thus, the pressure in the boundary layer is given by the classical perturbation in the outer solution due to the displacement thickness and the normal stress associated with the bulk viscosity; the latter is represented by the second term in (6.6). The perturbation in $\bar{p}$ due to the bulk viscosity can be written

$$\bar{\rho}\hat{\Delta} \approx \delta \bar{\mu}_b(\rho_0, \theta_0) \left(\frac{\partial u_0}{\partial \bar{\xi}} + \frac{\partial w_0}{\partial \hat{n}} \right) \tag{6.7}$$

and will vary with both $\bar{\xi}$ and $\hat{n}$. Thus, when $\mu_b = O(\mu/\delta) = O(\mu Re^{1/2})$, the first-order pressure is no longer constant across the flat plate boundary layer. The mass equation and plate conditions (4.20) can be used to show that $\hat{\Delta} = 0$ at $\hat{n} = 0$. As a result, there is at least one local maximum or minimum in the $\bar{\rho}\hat{\Delta}$ versus $\hat{n}$ curve.

By substitution of (6.6) in (4.6), (4.7) and (4.24) we obtain the following reduced forms of the first-order boundary-layer equations:

$$\frac{\partial(\bar{\rho}u)}{\partial \bar{\xi}} + \frac{\partial(\bar{\rho}w)}{\partial \hat{n}} = O(\delta^2), \tag{6.8}$$

$$\bar{\rho}\left[u\frac{\partial u}{\partial \bar{\xi}}+w\frac{\partial u}{\partial \hat{n}}\right]+\delta\frac{\mathrm{d}P_1}{\mathrm{d}\bar{\xi}} = \frac{\partial}{\partial \hat{n}}\left(\bar{\mu}\frac{\partial u}{\partial \hat{n}}\right)+O(\delta^2), \tag{6.9}$$

$$\bar{\rho}\bar{c}_p\left[u\frac{\partial \bar{T}}{\partial \bar{\xi}}+w\frac{\partial \bar{T}}{\partial \hat{n}}\right] = E\bar{\mu}\left(\frac{\partial u}{\partial \hat{n}}\right)^2+\frac{1}{Pr}\frac{\partial}{\partial \hat{n}}\left(\bar{k}\frac{\partial \bar{T}}{\partial \hat{n}}\right)+E\delta\beta T u\frac{\mathrm{d}P_1}{\mathrm{d}\bar{\xi}} + E\delta\left[(\beta T-1)\widehat{\boldsymbol{v}\cdot\boldsymbol{\nabla}}(\bar{\rho}\hat{\Delta})+\widehat{\boldsymbol{\nabla}\cdot(\boldsymbol{v}\bar{\rho}\hat{\Delta})}\right]+O(\delta^2), \tag{6.10}$$

where the transverse component of the momentum equation (4.8) is satisfied automatically. The boundary conditions corresponding to (6.8)–(6.10) are the $v=0$ versions of (4.20)–(4.22) and

$$u\sim 1+\delta U_1(\bar{\xi},0),\quad \bar{\rho}\sim 1+\delta R_1(\bar{\xi},0),\quad \bar{T}\sim 1+\delta T_1(\bar{\xi},0) \tag{6.11a–c}$$

as $\hat{n}\to\infty$.

Because the outer flow is a uniform flow, it can be shown that the mass and momentum equations, equations (6.8) and (6.9), are of exactly the same form as those of the classical $\mu_b=O(\mu)$ first-order theory. The energy equation (6.10) differs from the classical first-order flat plate equation only through the last two terms shown in (6.10).

We conclude this section by computing the pressure variation (6.6). The detailed calculation of each term in (6.6) requires a detailed solution of the lowest-order version of the boundary-layer equations (6.8)–(6.11) which is recognized as the classical lowest-order boundary-layer solution for a flat plate. As a result, we employ a conventional Levy–Lees similarity transform to the lowest-order versions of (6.6)–(6.11) (Lees 1956). The second term in (6.6) may then be written

$$\bar{\rho}\hat{\Delta}=-\delta\bar{\mu}_b\frac{\beta T}{2\bar{\xi}}F\frac{\theta_0'}{\theta_0}, \tag{6.12}$$

where $\theta_0'\equiv \mathrm{d}\theta_0/\mathrm{d}\eta$, η is the Levy–Lees similarity variable

$$\eta\equiv\frac{1}{\sqrt{2\bar{\xi}}}\int_0^{\hat{n}}\rho_0\,\mathrm{d}\hat{n} \tag{6.13}$$

and $F=F(\eta)$ is the non-dimensional version of the stream function

$$\psi\equiv(2\rho_\infty\mu_\infty U\xi)^{1/2}F(\eta). \tag{6.14}$$

Relation (6.12) holds for arbitrary fluids. If the fluid is an ideal gas $\beta T=1$ and (6.12) simplifies slightly.

We denote the dimensional form of the boundary-layer and displacement thicknesses by $\delta L d(\bar{\xi})$ and $\delta L d^*(\bar{\xi})$, respectively. The scaled boundary layer thickness $d(\bar{\xi})$ is then given by inverting (6.13) to yield

$$d(\bar{\xi})\equiv\sqrt{2\bar{\xi}}\int_0^{\eta_e}\frac{1}{\rho_0}\,\mathrm{d}\eta, \tag{6.15}$$

where η_e is the value of the similarity variable at the edge of the boundary layer. In terms of the Levy–Lees similarity variable, the scaled version of the displacement thickness is given by

$$d^*(\bar{\xi})\equiv\sqrt{2\bar{\xi}}\int_0^{\infty}\left(\frac{1}{\rho_0}-F'\right)\mathrm{d}\eta. \tag{6.16}$$

If we approximate the integral in (6.16) by

$$\int_0^{\infty} \left(\frac{1}{\rho_0} - F' \right) \mathrm{d}\eta \approx \int_0^{\eta_e} \left(\frac{1}{\rho_0} - F' \right) \mathrm{d}\eta, \tag{6.17}$$

we have

$$d^* \simeq d - \sqrt{2\bar{\xi}} F(\eta_e). \tag{6.18}$$

Once the $d^* = d^*(\bar{\xi})$ is determined we may compute the pressure perturbation in the outer flow due to the displacement thickness. Because the lowest-order outer flow is a uniform flow, $W_0(\bar{\xi}, 0) = 0$ and it can be shown that $P_1(\bar{\xi})$ is determined by solving the thin airfoil equation subject to the boundary condition

$$W_1(\bar{\xi}, 0) = \frac{\mathrm{d}(d^*)}{\mathrm{d}\bar{\xi}} = \frac{d^*}{2\bar{\xi}}. \tag{6.19}$$

In the remainder of this section, we take the outer flow to be supersonic so that the pressure perturbation is given by

$$P_1(\bar{\xi}, 0) = \frac{1}{\sqrt{M_\infty^2 - 1}} \frac{\mathrm{d}(d^*)}{\mathrm{d}\bar{\xi}} \tag{6.20}$$

which yields the well-known result that the first-order pressure perturbation decreases as $\bar{\xi}^{-1/2}$ in a supersonic outer flow.

We now solve the Levy–Lees similarity equations to determine $F(\eta)$, $F'(\eta)$, $F''(\eta)$, $\theta_0(\eta)$, $\theta_0'(\eta)$, etc. for the special case of a perfect gas, i.e. an ideal gas with constant specific heats, a Prandtl number = 0.7 = constant, a shear viscosity which is linear in absolute temperature, and a freestream Mach number of $M_\infty = 2$. The value of η_e is determined by the condition $F'(\eta_e) \approx 0.99$. At a given $\bar{\xi}$, the value of P_1 is determined from (6.15)–(6.20). The variation of $\bar{\rho}\hat{\Delta}$ at a given $\bar{\xi}$ is then given by (6.12) once the Reynolds number and the value and variation of $\bar{\mu}_b$ is chosen. In the following examples, we use a Reynolds number of 30 000 and $\bar{\xi} = 5$.

For our first example, we consider an adiabatic wall and have plotted $\bar{p}/\delta P_1$ versus $\hat{n}/d$ in figure 3. The quantity $\bar{p}/\delta P_1$ is the pressure perturbation scaled with that due to the displacement thickness and is unity in the classical $\bar{\mu}_b = O(1)$ first-order theory. The quantity $\hat{n}/d$ is recognized as also equal to the dimensional n-coordinate divided by the dimensional boundary-layer thickness. Each curve in figure 3 corresponds to a constant value of $\bar{\mu}_b$. Values of $\bar{\mu}_b$ were taken to be 0, 100, 200, 300, 400 and 500. Because $\bar{\mu}_b$ is constant with $\hat{n}$, the variation in $\bar{p}/\delta P_1$ reflects the variation in $\widehat{\boldsymbol{\nabla} \cdot \boldsymbol{v}}$, i.e. the coefficient of $\delta\bar{\mu}_b$ in (6.12). For the adiabatic plate, the temperature $\theta_0 = \theta_0(\eta)$ decreases monotonically with increasing η or $\hat{n}$ and $\bar{p}/\delta P_1 - 1$ is always positive. We also note that the disturbance in $\bar{p}$ is non-zero outside of the momentum boundary layer. Inspection of (6.12) reveals that $\overline{\rho}\hat{\Delta}$ only goes to zero outside of the temperature boundary layer, i.e. only as $\theta_0' \to 0$.

In the simple case of an adiabatic plate, perfect gas, constant Prandtl number and Chapman–Rubesin parameter equal to unity,

$$F = F(\eta), \tag{6.21}$$

$$\theta_0 = \theta_0(\eta; Pr, E) = 1 + E\tilde{\theta}_0(\eta; Pr). \tag{6.22}$$

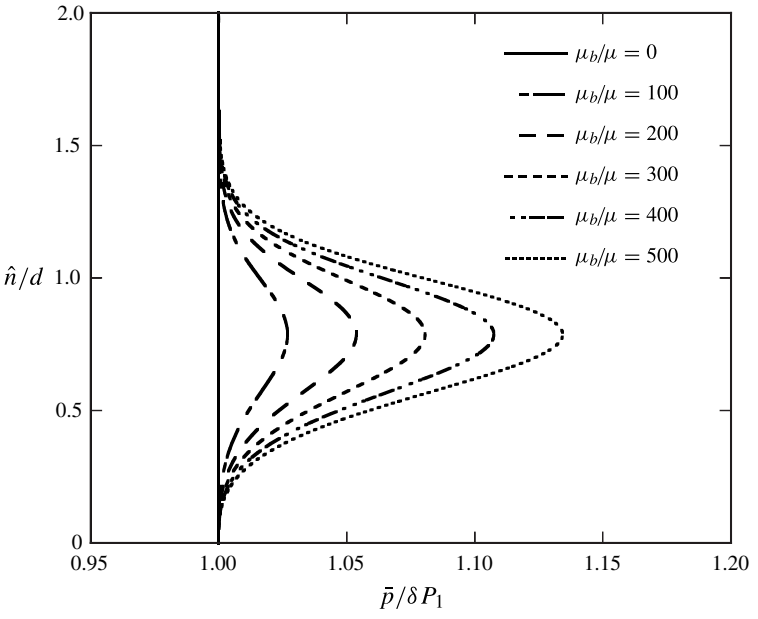

FIGURE 3. Variation of the pressure perturbation (6.6) for various values of μ_b/μ. The gas is perfect, $Re = 3 \times 10^4$, $Pr = 0.7$, $\gamma = 1.4$ and $M_\infty = 2$.

Thus, the Eckert number $E = U^2/c_{p\infty}T_\infty = M_\infty^2(\gamma - 1)$ can be scaled out to yield a simplified version of (6.12):

$$\bar{\rho}\hat{\Delta} = -\frac{\delta\bar{\mu}_b}{2\xi}F\frac{E\tilde{\theta}_0'}{1 + E\tilde{\theta}_0}. \tag{6.23}$$

If we also take $\bar{\mu}_b = \text{constant}$ the dependence of $\bar{\rho}\hat{\Delta}$ on Mach number is therefore obtained explicitly. For this simple case, $\bar{\rho}\hat{\Delta}$ grows roughly linearly with increasing M_∞^2, particularly when $\gamma \approx 1$. Because d, d^* and P_1 will vary with E, there will be a redistribution and further stretching of $\bar{p}/\delta P_1$ with M_∞^2. For the case of $\bar{\mu}_b = 500$ we have plotted the variation of $\bar{p}/\delta P_1$ with $\hat{n}/d$ for various values of M_∞ in figure 4.

In figure 5, we have plotted the variation of $\bar{p}/\delta P_1$ versus $\hat{n}/d$ for heated and cooled plates for $\bar{\mu}_b = 500 = \text{constant}$. As a reference, the case of an adiabatic plate is also included. In the case of heated walls, i.e. the cases of $\theta_w = 1.0$ and 1.5, θ_0 has a local maximum which, from (6.12), requires that $\bar{\rho}\hat{\Delta} = 0$ at the local maximum of θ_0. Thus, $\bar{p}/\delta P_1 - 1$ will change sign for heated walls.

As discussed by Cramer (2012), the value of μ_b can vary significantly with temperature. As a result, the variation of $\bar{p}/\delta P_1$ will, in general, differ from that predicted by a calculation using constant μ_b. To illustrate the differences possible, we consider the case of methane (CH_4). Below 260 K, the primary contribution to the bulk viscosity of CH_4 is the rotational mode resulting in $\mu_b = O(\mu)$ and a weak increase in μ_b with temperature (Cramer 2012). At higher temperatures, the vibrational mode is dominant yielding bulk viscosities which are hundreds of times larger than the shear viscosity. The temperature variation of the dimensional bulk viscosity of CH_4 has been plotted in figure 6. From 100 to 300 K, the power law fit for the rotational mode as given by Cramer (2012) is used. The rotational contribution

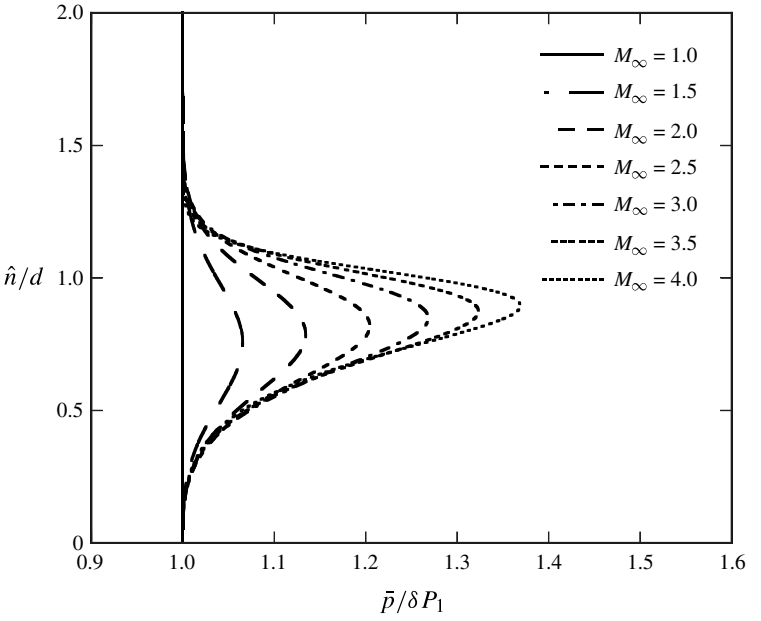

FIGURE 4. Variation of the pressure perturbation (6.6) for various values of freestream Mach number. The gas is perfect, $Re = 3 \times 10^4$, $Pr = 0.7$, $\gamma = 1.4$ and $\bar{\mu}_b = 500$.

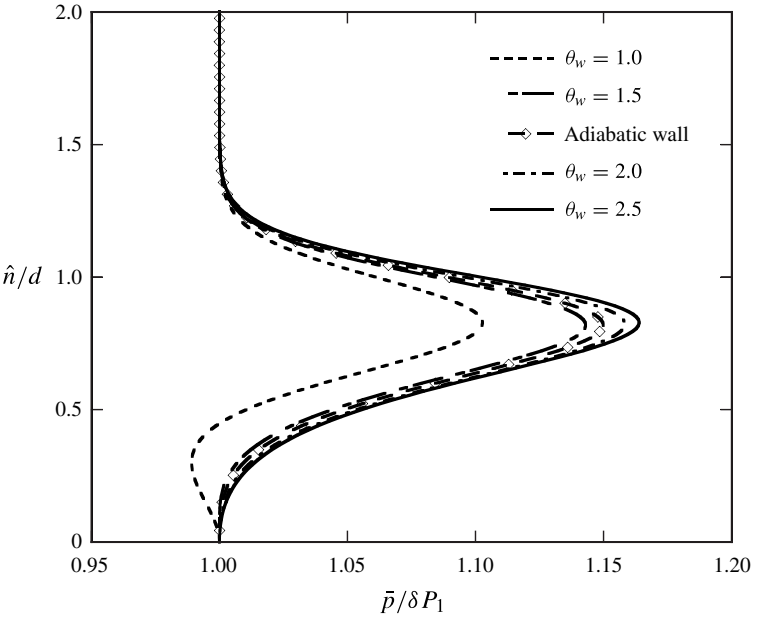

FIGURE 5. Effect of wall heating or cooling on the pressure perturbation (6.6). The gas is perfect, $Re = 3 \times 10^4$, $Pr = 0.7$, $\gamma = 1.4$, $\bar{\mu}_b = 500$ and $M_\infty = 2$.

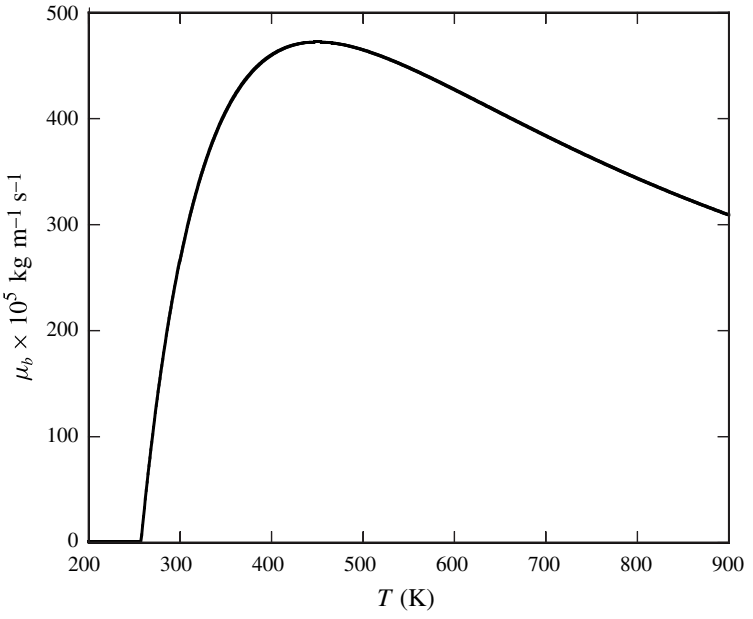

FIGURE 6. Variation of the bulk viscosity of methane with temperature.

is set equal to zero for $T > 300$ K. Below approximately 260 K, the vibrational mode is deactivated and the vibrational contribution is set equal to zero. Above 260 K the vibrational portion of the bulk viscosity is computed from the Landau–Teller fit given by equation (30) of Cramer (2012) and is added to the rotational contribution. At 300 K, there will be a relatively small discontinuity in μ_b. However, at 300 K the vibrational contribution is much larger than the rotational contribution and the discontinuity will have no significant impact on the following plots or discussion.

In figure 7, we compare the scaled boundary-layer pressure using the variable μ_b of figure 6 to that computed with a constant μ_b. As in the previous calculations we take the gas to be perfect with $Pr = 0.7$, a shear viscosity proportional to temperature and a freestream Mach number of 2. The plate is taken to be adiabatic. The freestream Reynolds number is 30 000 and $\bar{\xi} = 5$. The ratio of specific heats is computed from the freestream temperature and the data and correlations of Reid, Prausnitz & Poling (1987). In the cases computed using a constant μ_b, the freestream bulk viscosity ($\mu_{b\infty}$) is used. When $T_\infty = 200$ K, $\gamma_\infty \equiv 1.4$ and the vibrational mode is not activated in the freestream. As a result, $\mu_b = O(\mu)$ in the freestream and $\bar{p}/\delta P_1 \approx 1$ when a constant μ_b is used. However, the wall temperature is approximately 328 K resulting in a layer of large bulk viscosity fluid near the wall. As seen in figure 7 the computed pressure perturbation deviates significantly from that of the constant μ_b case below $\hat{n} = 0.6d$. At freestream temperatures of 300 and 400 K $\mu_b \gg \mu$ throughout the boundary layer and $\bar{p}/\delta P_1$ is of the same general size as seen in the previous calculations regardless of whether a variable or constant bulk viscosity is used. When $T_\infty = 300$ K, $\gamma_\infty \equiv 1.3$ and the wall temperature is 452 K which is approximately the local maximum in μ_b seen in figure 6. Thus, the bulk viscosity is always larger than the freestream value and the pressures are noticeably larger than those computed with $\mu_b = \mu_{b\infty}$. When $T_\infty = 400$ K, $\gamma_\infty \equiv 1.25$ and the wall temperature is approximately 569 K. Inspection of figure 6 reveals that the bulk viscosities in the boundary layer are always

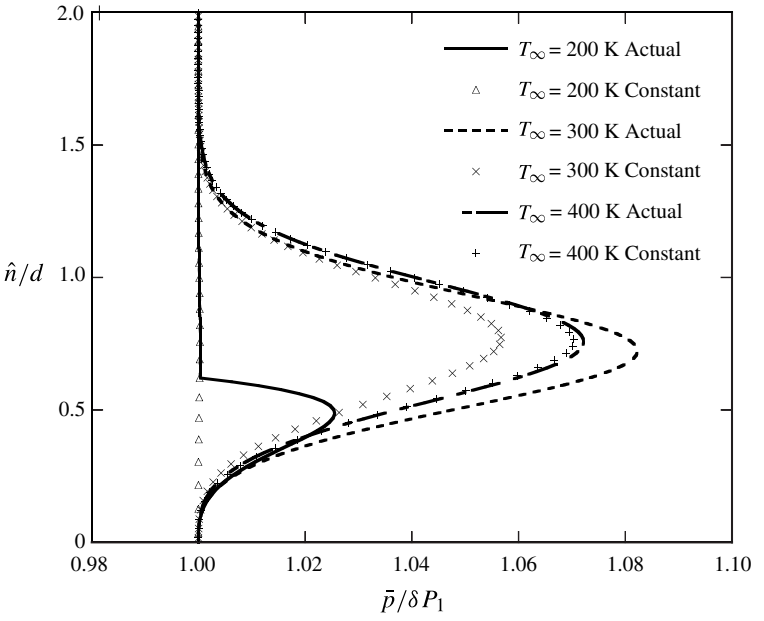

FIGURE 7. Effect of temperature variation of μ_b. The gas is perfect, the plate is adiabatic, $Re = 3 \times 10^4$, $Pr = 0.7$ and $M_\infty = 2$. The ratio of specific heats is constant and taken to be the value at the freestream.

near the local maximum of μ_b. As a result, there is little difference between the pressures based on constant μ_b and those based on variable μ_b. When the freestream temperature is larger than approximately 450 K, the bulk viscosity in the boundary layer will always be less than the freestream value. At these temperatures the pressure levels in an actual boundary layer will always be less than those computed with $\mu_b = \mu_{b\infty}$.

Further description of the effects of large bulk viscosity on the skin friction and heat transfer for the simplest case of a flat plate and a steady flow will require detailed numerical solutions of (6.8)–(6.11). Owing to the first-order pressure gradient in (6.9) and the first-order source terms in (6.10), the boundary layer will be non-similar. However, solutions to (6.10) will clearly depend on the bulk viscosity even in the simplest cases. Thus, we expect the first-order temperature perturbation θ_1, heat transfer coefficient and recovery factor will also have a dependence on the large bulk viscosity. The momentum equation (6.9) is coupled to the temperature equation (6.10) through the temperature dependencies of the viscosity and density. For the weak pressure gradient of (6.9), the coupling is primarily through the Chapman–Rubesin parameter $C \equiv \bar{\rho}\bar{\mu}$ (White 1974). If we employ (4.26) and (6.6) and adopt a power law model for the shear viscosity, i.e. $\mu \propto T^q$, we find that

$$C = \theta_0^{q-1}\left\{1 + \delta\left[(q-1)\frac{\theta_1}{\theta_0} + P_1 + \overline{\rho}\hat{\Delta}\right] + O\left(\delta^2\right)\right\}, \tag{6.24}$$

at every ξ, η. At the plate, i.e. at $\hat{n} = 0$, $\hat{\Delta} = 0$ and

$$C_w = \theta_{ow}^{q-1}\left\{1 + \delta\left[(q-1)\frac{\theta_{1w}}{\theta_{ow}} + P_1\right] + O\left(\delta^2\right)\right\}. \tag{6.25}$$

The subscripts w refer to quantities evaluated at $\hat{n}=0$. Thus, the velocity distribution is expected to be affected by the large bulk viscosity over major portions of the boundary layer, regardless of the viscosity law used. At the plate C_w will be influenced by μ_b indirectly through θ_1 which, in turn, is affected by the source terms in (6.10) provided $q \neq 1$. As mentioned above, more precise characterizations of these corrections will require detailed numerical calculations; such calculations will be the focus of future studies.

7. Summary

We have examined steady large-Reynolds-number flows of fluids having bulk viscosities which are much greater than their shear viscosities. The freestream Mach number was taken to be of order one and our general results are valid for three-dimensional flows. Throughout this study the boundary layers were taken to be laminar and attached. When the ratio of bulk to shear viscosity is of the order of the square root of the Reynolds number, the lowest order outer and boundary-layer flow remain unaffected but the first corrections to the flows in both regions must include the effects of bulk viscosity. This contrasts with the $\mu_b = O(\mu)$ theory in which the effects of bulk viscosity are negligible even at first order.

In the outer flow the effects of bulk viscosity are of the same order as the corrections due to the displacement thickness. The resultant first-order flow is seen to have non-uniform entropy and to be frictional and rotational. In spite of the presence of longitudinal friction, the first-order flow can be computed by allowing slip at solid surfaces. In § 3 we have shown that the Bernoulli constant, i.e. the stagnation enthalpy, will be perturbed by an amount equal to $\Delta \equiv \nu_b \boldsymbol{\nabla} \cdot \boldsymbol{v}$.

In the boundary layer the primary new effects of the large bulk viscosity are the presence of two source terms in the temperature equation and the necessity of a variation of the thermodynamic pressure across the boundary layer. In the simplest case of a flat plate boundary layer, it is the first-order normal stress which is constant across the boundary layer rather than the first-order pressure.

The results described here are relatively easy to achieve in practice. For example, if the freestream Reynolds number is 250 000, the effects of bulk viscosity ought to be observed in sufficiently accurate calculations or experiments for fluids having $\mu_b = 0(500\mu)$. Inspection of figure 1 and further results presented by Cramer (2012) reveal that many common fluids have bulk viscosities in this range at room temperatures and pressures.

Acknowledgement

This work was supported by National Science Foundation grant CBET-0625015.

REFERENCES

BAHMANI, F. 2013 Three problems involving compressible flow with large bulk viscosity and non-convex equations of state. PhD thesis, Virginia Polytechnic Institute and State University, Blacksburg, Virginia.

CRAMER, M. S. 2012 Numerical estimates for the bulk viscosity of ideal gases. *Phys. Fluids* **24**, 066102.

EMANUEL, G. 1992 Effect of bulk viscosity on a hypersonic boundary layer. *Phys. Fluids* A **4** (3), 491–495.

GONZALEZ, H. & EMANUEL, G. 1993 Effect of bulk viscosity on Couette flow. *Phys. Fluids* A **5**, 1267–1268.

GRAVES, R. E. & ARGROW, B. A. 1999 Bulk viscosity: past to present. *Intl J. Thermophys.* **13** (3), 337–342.

LEES, L. 1956 Laminar heat transfer over blunt-nosed bodies at hypersonic speeds. *Jet Propul.* **26**, 259–269.

REID, R. C., PRAUSNITZ, J. M. & POLING, B. E. 1987 *The Properties of Gases and Liquids*. Wiley.

TISZA, L. 1942 Supersonic absorption and Stokes' viscosity relation. *Phys. Rev.* **61**, 531–536.

VAN DYKE, M. 1964 *Perturbation Methods in Fluid Mechanics*. Academic Press.

WHITE, F. M. 1974 *Viscous Fluid Flow*. McGraw-Hill.